Hindawi
Shock and Vibration
Volume 2021, Article ID 1219429, 17 pages
https://doi.org/10.1155/2021/1219429

Research Article

Influence of Variable Nonlocal Parameter and Porosity on the Free Vibration Behavior of Functionally Graded Nanoplates

Pham Van Vinh[1] **and Le Quang Huy**[2]

[1]*Department of Solid Mechanics, Le Quy Don Technical University, 236 Hoang Quoc Viet, Hanoi, Vietnam*
[2]*Institute of Techniques for Special Engineering, Le Quy Don Technical University, 236 Hoang Quoc Viet, Hanoi, Vietnam*

Correspondence should be addressed to Pham Van Vinh; phamvanvinh@lqdtu.edu.vn

Received 19 April 2021; Revised 19 June 2021; Accepted 23 June 2021; Published 15 July 2021

Academic Editor: Zhaoye Qin

Copyright © 2021 Pham Van Vinh and Le Quang Huy. This is an open access article distributed under the Creative Commons Attribution License, which permits unrestricted use, distribution, and reproduction in any medium, provided the original work is properly cited.

This paper studies the influence of the variable nonlocal parameter and porosity on the free vibration behavior of the functionally graded nanoplates with porosity. Four patterns of distribution of the porosity through the thickness direction are considered. The classical nonlocal elasticity theory is modified to take into account the variation of the nonlocal parameter through the thickness of the nanoplates. The governing equations of motion are established using simple first-order shear deformation theory and Hamilton's principle. The closed-form solution based on Navier's technique is employed to solve the governing equations of motion of fully simply supported nanoplates. The accuracy of the present algorithm is proved via some comparison studies in some special cases. Then, the effects of the porosity, the variation of the nonlocal parameter, the power-law index, aspect ratio, and the side-to-thickness ratio on the free vibration of nanoscale porous plates are investigated carefully. The numerical results show that the porosity and nonlocal parameter have strong effects on the free vibration behavior of the nanoplates.

1. Introduction

The applications of micro/nanostructures in the micro/nanoelectromechanical system (MEMS and NEMS) are increasing rapidly based on the development of micro/nanotechnology, structures, and materials. At the micro/nanodimension, the small-scale effects on the thermal and mechanical behaviors of micro/nanostructures cannot be neglected. To address this problem, molecular dynamics (MD) can be served as an excellent method to predict the exact behavior of the micro/nanostructures, but the MD usually costs expensive computation. Therefore, many researchers have been focused on developing higher-order continuum theory to analyze small-scale structures, for instance, the couple stress theory and modified couple stress theory [1–4], the nonlocal elasticity theory [5–7], and strain gradient theory and nonlocal strain gradient theory [8–13]. More details on these theories and their applications can be read from the literature review of Thai et al. [14]. Among them, the nonlocal elasticity theory which is first established by Eringen is usually used in combination with shear deformation theories by many scientists to analyze nanoplates, nanobeams, and nanoshells. Many remarkable works on the analysis of nanostructures can be reviewed herein. Zhang et al. [15] analyzed the buckling of multiwalled carbon nanotubes under compression with small-scale effects. Hu et al. [16] developed a nonlocal shell model to analyze wave propagation in single- and double-walled carbon nanotubes. The free vibration of multiwalled carbon nanotubes embedded in an elastic foundation has been analyzed by Li and Kardomateas [17] using a nonlocal elastic shell model. Wang and Varadan [18] employed nonlocal elastic shell theory to analyze the wave propagation of carbon nanotubes. Rouhi and Ansari [19] developed a nonlocal Flugge shell model to study the axial buckling of double-walled carbon nanotubes with different end conditions. Pradhan and Phadikar [20] investigated the small-scale effect on the vibration of multilayered graphene sheets resting on an elastic foundation using nonlocal continuum models. Aksencer and Aydogdu [21] analyzed the vibration and buckling of nanoplates using

nonlocal elasticity theory and Levy type solution. Shen et al. [22] investigated the free vibration of a single-layered graphene sheet-based nanomechanical sensor using nonlocal Kirchhoff plate theory. Zhang et al. [23, 24] applied nonlocal elasticity theory to analyze free vibration and buckling of single-layered graphene sheets based on the kp-Ritz method. Ansari et al. [25, 26] analyzed single- and multilayered graphene sheets using nonlocal elasticity theory. Hosseini-Hashemi et al. [27] developed an exact solution for free vibration of functionally graded circular/annular Mindlin nanoplates using nonlocal elasticity theory. Anjomshoa and Tahani [28] analyzed the free vibration of orthotropic circular and elliptical nanoplates resting on elastic foundations. Fatima et al. [29] developed a nonlocal zeroth-order shear deformation theory for free vibration of functionally graded nanoplates. Zenkour et al. [30–32] analyzed the thermal buckling and bending of orthotropic carbon nanotubes using nonlocal elasticity theory and mixed variation formula. Aghababaei and Reddy [33] developed a nonlocal third-order shear deformation theory to analyze bending and free vibration of nanoplates. Ansari and Sahmani [34] analyzed the buckling behavior of single-layered graphene sheets using a nonlocal plate model and MD simulations. Hosseini-Hashemi et al. [35] employed an analytical solution to study the buckling and free vibration of nanoplates via nonlocal third-order shear deformation theory. Daneshmehr et al. [36, 37] analyzed stability and free vibration of functionally graded nanoplates via nonlocal elasticity theory and higher-order shear deformation theory. Malezadeh and Shojaee [38] developed a nonlocal two-variable refined plate theory to analyze the free vibration of nanoplates. Narendar and Gopalakrishnan [39, 40] applied a combination of two-variable shear deformation theory and nonlocal elasticity theory to analyze buckling of micro/nanoplates. Hoa et al. [41] established a novel nonlocal higher-order with only one unknown variable to analyze the bending and free vibration of functionally graded nanoplates. Sobhy and Zenkour [42–46] and Zenkour and Sobhy [47] developed several nonlocal shear deformation theories to analyze single-, double-, and multilayered graphene sheets as well as orthotropic nanoplates with and without elastic foundations. Thai et al. [48] developed a nonlocal sinusoidal plate theory to study micro/nanoplates. Fattahi et al. [49] applied nonlocal elasticity theory to determine vibrational behavior of FGM nanoplates. Sahmani and Safaei [50] studied the large-amplitude oscillations of composite conical nanoshells considering surface stress effect. To take into account the thickness stretching effects, Sobhy and Radwan [51] developed a new quasi-3D nonlocal plate theory to investigate the vibration and buckling behavior of functionally graded nanoplates. Bessaim et al. [52] established a nonlocal quasi-3D trigonometric plate theory for free vibration analysis of micro/nanoplates.

Functionally graded materials (FGMs) were first introduced by some Japanese's scientists in the 1950s. Due to their high performance, they have been used widely in many files of engineering, industry, and other special areas of engineering [53, 54]. These materials also applied to produce micro/nanostructures. It is noticed that the porosity usually occurs during the process of manufacture and/or they can be created intentionally to reduce the mass of the structures and control the vibration of the structures. In the case of attended creation, the print-3D technology can be used to create porous structures with desired distribution of porosity. Therefore, numerous works have been done on the investigation of free and forced vibration of FGM macro/micro/nanoplates with and without porosity. Rezaei et al. [55] analyzed the free vibration of FGM plates with porosity using a simple four-variable plate theory. Riadh et al. [56] used a higher-order and normal shear deformation theory to analyze the free vibration response of FGM porous plates. The vibration analysis of temperature-dependent FGM beams with porosity was investigated by Ebrahimi and Jafari [57]. Gao et al. [58] studied wave propagation in FGM porous plates reinforced with graphene platelets in which Young's modulus and mass density depend on the porosity distribution through the thickness of the plates, while Poisson's ratio does not depend on the porosity. Moradi-Dastjerdi et al. [59–61] analyzed thermo-electro-mechanical, free vibration, and buckling behaviors of advanced smart sandwich plates including the effects of porosity. In these studies, Young's modulus, mass density, and Poisson's ratio are assumed to depend on the individual material properties and porosity. Akbaş et al. [62] examined the bending and vibration of FGM nanoplates with porosity. Wattanasakulpong and Ungbhakorn [63] studied the linear and nonlinear vibration of elastically restrained ends of FGM beams with porosity. Allahkarami et al. [64] examined the dynamic stability of bidirectional FGM cylindrical shells with porosity. Fan et al. [65] used a modified couple stress theory to analyze geometrically nonlinear vibration of FGM microplates with porosity. The effects of porosity on the free vibration of FGM nanoplates resting on Winkler–Pasternak elastic foundation were investigated by Mechab and his coworkers [66]. Shahverdi and Barati [67] analyzed the free vibration of porous FGM nanoplates. Barati and Shahverdi [68] analyzed forced vibration of FGM nanoplates with porosity under dynamic load using a general nonlocal stress-strain gradient theory. Shahsavari et al. [69] analyzed the shear buckling behavior of nanoplates with porosity using a new size-dependent quasi-3D theory. Daikh et al. [70] investigated the buckling behavior of FGM sandwich nanoplates with porosity with the effects of heat conduction via nonlocal strain gradient theory.

According to the literature review, most studies on the mechanical behavior of FGM nanoplates with and without porosity are carried out based on the nonlocal elasticity theory with a constant nonlocal parameter. On the other hand, it is obvious that the nonlocal parameter depends on the material components. So, it is necessary to consider the variation of the nonlocal parameter on the mechanical analysis of FGM nanoplates. This is the main aim of the present study, in which the classical Eringen's elasticity theory is modified to consider the variable nonlocal parameter for free vibration analysis of FGM porous nanoplates. In addition, the effects of the porosity, the side-to-thickness ratio, and the aspect ratio incorporating with variable nonlocal parameter are studied cautiously.

2. Material Properties of FGM Nanoplates with Porosity

A rectangular FGM nanoplate with porosity is considered. The dimensions of the plate are $a \times b$, and the thickness is h. The Cartesian coordinate xyz is placed at the middle surface of the FGM nanoplates as shown in Figure 1.

The distribution of the ceramic and metal components through the thickness of the plate is described via the volume fractions with the power-law function. The porosity is distributed through the thickness of the plate with four different patterns, namely, patterns A, B, C, and D, and they are described by the following formula [58, 71]:

$$p(z) = \begin{cases} P_0 \cos\left(\dfrac{\pi z}{h}\right), & \text{for pattern A,} \\ P_0\left[1 - \cos\left(\dfrac{\pi z}{h}\right)\right], & \text{for pattern B,} \\ P_0 \cos\left(\dfrac{\pi z}{2h} + \dfrac{\pi}{4}\right), & \text{for pattern C,} \\ P_0 \cos\left(\dfrac{\pi z}{2h} - \dfrac{\pi}{4}\right), & \text{for pattern D,} \end{cases} \tag{1}$$

where $P_0 \le 0.5$ is the maximum porosity value [72]. The effective Young's modulus, shear modulus, and mass density can be calculated as the following formula [58, 71]:

$$\begin{aligned} E(z) &= \widetilde{E}(z)[1 - p(z)], \\ \rho(z) &= \widetilde{\rho}(z)[1 - p(z)], \\ G(z) &= \frac{E(z)}{2(1 - \nu(z))}, \\ \mu(z) &= \widetilde{\mu}(z), \end{aligned} \tag{2}$$

where $\widetilde{E}(z), \widetilde{\rho}(z), \nu(z)$, and $\widetilde{\mu}(z)$ are the effective Young's modulus, mass density, Poisson's ratio, and nonlocal parameter of the perfect FGM nanoplates; they are calculated via the power-law function as follows [58, 71, 73]:

$$\begin{aligned} \widetilde{E}(z) &= E_m + (E_c - E_m)\left(\frac{z}{h} + \frac{1}{2}\right)^k, \\ \widetilde{\rho}(z) &= \rho_m + (\rho_c - \rho_m)\left(\frac{z}{h} + \frac{1}{2}\right)^k, \\ \nu(z) &= \nu_m + (\nu_c - \nu_m)\left(\frac{z}{h} + \frac{1}{2}\right)^k, \\ \widetilde{\mu}(z) &= \mu_m + (\mu_c - \mu_m)\left(\frac{z}{h} + \frac{1}{2}\right)^k, \end{aligned} \tag{3}$$

where k is a nonnegative power-law index. In this study, the FGM nanoplates are made of mixture of several individual components. The material properties of these individual components are given in Table 1. Figure 2 presents the dispersion of porosity and effective material properties of the Al/ZrO_2 FGM nanoplates with $k = 3$. Figure 2(a) displays the normalized distribution of porosity through the thickness of the plates. Figures 2(b) and 2(c) plot the variation of the effective Young's modulus and mass density of the material through the thickness direction of the nanoplates. The variation of the effective nonlocal parameter of the material through the thickness of the nanoplates with $\mu_m = 2$ and different values of nonlocal parameter's ratio μ_c/μ_m is presented in Figure 2(d).

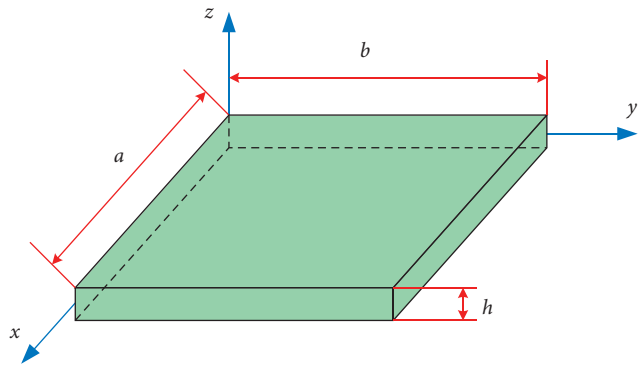

Figure 1: The geometric model of FGM porous nanoplates.

3. Theoretical Formulation

3.1. Simple First-Order Shear Deformation Theory

3.1.1. Kinematic. In this study, a simple first-order shear deformation theory (S-FSDT) which was introduced by Thai and Choi [74, 75] is used to describe the kinematics of the nanoplates. The displacement field of this theory can be written as the following formula:

$$\begin{aligned} u(x, y, z, t) &= u(x, y, t) - z\frac{\partial w_b}{\partial x}, \\ v(x, y, z, t) &= v(x, y, t) - z\frac{\partial w_b}{\partial y}, \\ w(x, y, z, t) &= w_b(x, y, t) + w_s(x, y, t). \end{aligned} \tag{4}$$

The strain fields of the plate are obtained as

$$\begin{aligned} \begin{Bmatrix} \varepsilon_x \\ \varepsilon_y \\ \gamma_{xy} \end{Bmatrix} &= \begin{Bmatrix} \varepsilon_x^0 \\ \varepsilon_y^0 \\ \gamma_{xy}^0 \end{Bmatrix} + z\begin{Bmatrix} \kappa_x \\ \kappa_y \\ \kappa_{xy} \end{Bmatrix}, \\ \begin{Bmatrix} \gamma_{xz} \\ \gamma_{yz} \end{Bmatrix} &= \begin{Bmatrix} \gamma_{xz}^0 \\ \gamma_{yz}^0 \end{Bmatrix}, \end{aligned} \tag{5}$$

where

Table 1: Material properties of some individual metal/ceramic components.

Materials	Al	SUS304	Al_2O_3	Si_3N_4	ZrO_2
Young's modulus (GPa)	70	201.04	380	348.43	200
Mass density (kg/m^3)	2707	8166	3800	2370	5700
Poisson's ratio	0.3	0.3	0.3	0.24	0.3
Nonlocal parameter	2	2	—	—	—

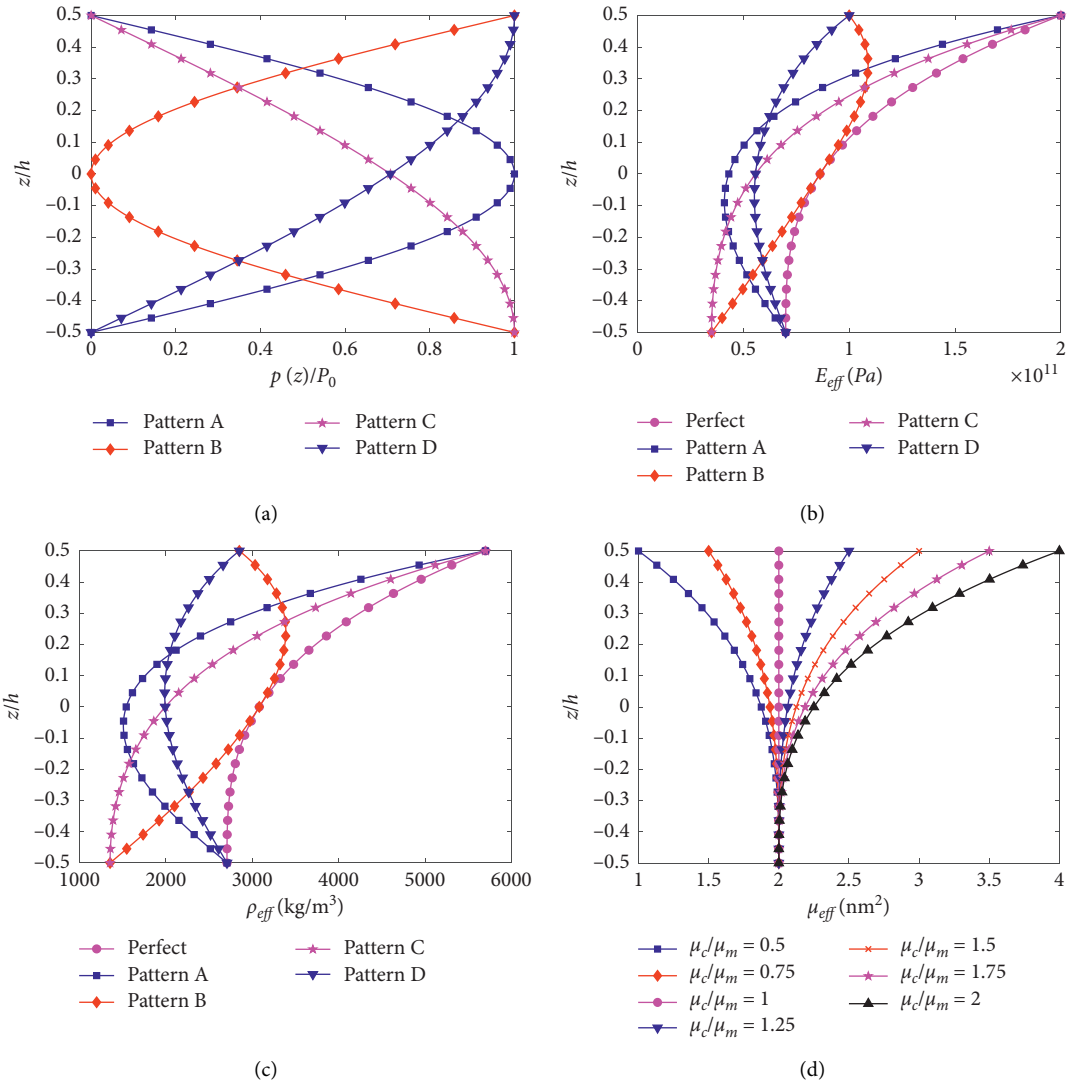

Figure 2: The distribution of porosity and effective material properties of Al/ZrO_2 FGM nanoplates: (a) distribution of porosity; (b) $k = 3, 0$, $P_0 = 0.5$; (c) $k = 3, 0$, $P_0 = 0.5$; (d) $k = 3$.

$$\begin{Bmatrix} \varepsilon_x^0 \\ \varepsilon_y^0 \\ \gamma_{xy}^0 \end{Bmatrix} = \begin{Bmatrix} \dfrac{\partial u}{\partial x} \\ \dfrac{\partial v}{\partial y} \\ \dfrac{\partial u}{\partial y} + \dfrac{\partial v}{\partial x} \end{Bmatrix},$$

$$\begin{Bmatrix} \kappa_x \\ \kappa_y \\ \kappa_{xy} \end{Bmatrix} = -\begin{Bmatrix} \dfrac{\partial^2 w_b}{\partial x^2} \\ \dfrac{\partial^2 w_b}{\partial y^2} \\ 2\dfrac{\partial^2 w_b}{\partial x\, \partial y} \end{Bmatrix}, \tag{6}$$

$$\begin{Bmatrix} \gamma_{xz}^0 \\ \gamma_{yz}^0 \end{Bmatrix} = \begin{Bmatrix} \dfrac{\partial w_s}{\partial x} \\ \dfrac{\partial w_s}{\partial y} \end{Bmatrix}.$$

3.1.2. The Relations of Constitutive. The constitutive equations of the plate are expressed as

$$\begin{Bmatrix} \sigma_x \\ \sigma_y \\ \tau_{xy} \end{Bmatrix} = \begin{bmatrix} C_{11} & C_{12} & 0 \\ C_{12} & C_{22} & 0 \\ 0 & 0 & C_{66} \end{bmatrix} \begin{Bmatrix} \varepsilon_x \\ \varepsilon_y \\ \gamma_{xy} \end{Bmatrix}, \tag{7}$$

$$\begin{Bmatrix} \tau_{xz} \\ \tau_{yz} \end{Bmatrix} = \begin{bmatrix} C_{55} & 0 \\ 0 & C_{44} \end{bmatrix} \begin{Bmatrix} \gamma_{xz} \\ \gamma_{yz} \end{Bmatrix}, \tag{8}$$

where

$$C_{11} = C_{22} = \frac{E(z)}{1 - \nu(z)^2},$$

$$C_{12} = \nu(z) C_{11}, \tag{9}$$

$$C_{44} = C_{55} = C_{66} = \frac{E(z)}{2(1 + \nu(z))}.$$

3.2. The Nonlocal Elasticity Theory. In Eringen's nonlocal elasticity theory [5–7], the stress at any point in a continuum body depends on the strains at all neighbor points. The differential form of the classical nonlocal elasticity theory of Eringen is as the following formula [7]:

$$\left(1 - \mu\nabla^2\right)\sigma_{ij} = t_{ij}, \tag{10}$$

where σ_{ij} and t_{ij} are, respectively, the nonlocal and local stress tensors, $\nabla^2 = \partial^2/\partial x^2 + \partial^2/\partial y^2$ is the second Laplace operator, and $\mu = (e_0 l)^2\,(\mathrm{nm}^2)$ is the nonlocal parameter, in which e_0 is a material constant which is determined via experimental or atomistic dynamics and l is an internal characteristic length. It is obvious that the nonlocal parameter of classical Eringen's theory is assumed to be constant. However, it can be seen that e_0 and l are two material-dependent parameters, so the nonlocal parameter μ should be a material-dependent parameter. Consequently, it is necessary to consider the variation of the nonlocal parameter through the thickness of FGM nanoplates. In this study, the nonlocal parameter is assumed to vary through the thickness direction of the FGM nanoplates. Hence, the nonlocal constitutive relations of the plates can be modified as follows:

$$\begin{Bmatrix} t_x \\ t_y \\ t_{xy} \end{Bmatrix} = \left(1 - \mu(z)\nabla^2\right) \begin{Bmatrix} \sigma_x \\ \sigma_y \\ \tau_{xy} \end{Bmatrix} = \begin{bmatrix} C_{11} & C_{12} & 0 \\ C_{12} & C_{22} & 0 \\ 0 & 0 & C_{66} \end{bmatrix} \begin{Bmatrix} \varepsilon_x \\ \varepsilon_y \\ \gamma_{xy} \end{Bmatrix}, \tag{11}$$

$$\begin{Bmatrix} t_{yz} \\ t_{xz} \end{Bmatrix} = \left(1 - \mu(z)\nabla^2\right) \begin{Bmatrix} \tau_{yz} \\ \tau_{xz} \end{Bmatrix} = \begin{bmatrix} C_{44} & 0 \\ 0 & C_{55} \end{bmatrix} \begin{Bmatrix} \gamma_{yz} \\ \gamma_{xz} \end{Bmatrix}. \tag{12}$$

3.3. Equations of Motion. The equations of motion are achieved via Hamilton's principle as follows:

$$0 = \int_0^T (\delta U - \delta K)\mathrm{d}t, \tag{13}$$

where δU is the variation of the strain energy and δK is the variation of the kinematic energy of the plate. The variation of the strain energy is obtained as the following expression [33, 35]:

$$\delta U = \int_A \int_{-h/2}^{h/2} \left(\sigma_x \delta\varepsilon_x + \sigma_y \delta\varepsilon_y + \tau_{xy}\delta\varepsilon_{xy} + \tau_{xz}\delta\varepsilon_{xz} + \tau_{yz}\delta\varepsilon_{yz}\right)\mathrm{d}z\mathrm{d}A. \tag{14}$$

The variation of the kinematic energy of the plate is expressed as [33, 35]:

$$\delta K = \int_A \int_{-h/2}^{h/2} (\dot{u}\delta\dot{u} + \dot{v}\delta\dot{v} + \dot{w}\delta\dot{w})\rho(z)\mathrm{d}z\mathrm{d}A. \tag{15}$$

By substituting equations (7) and (8) into equation (14), inserting equation (4) into equation (15), and considering the nonlocal relations of equations (11) and (12), after integrating through the thickness of the plates, the governing equations of motion of the sandwich plates are derived from equation (13) as the following formulas:

$$\delta u\colon \frac{\partial N_x}{\partial x}+\frac{\partial N_{xy}}{\partial y}$$

$$\delta v\colon \frac{\partial N_y}{\partial y}+\frac{\partial N_{xy}}{\partial x}=I_0\ddot{v}-I_1\frac{\partial \ddot{w}_b}{\partial y}-\nabla^2\left(L_0 v-L_1\frac{\partial \ddot{w}_b}{\partial y}\right),$$

$$\delta w_b\colon \frac{\partial^2 M_x}{\partial x^2}+2\frac{\partial^2 M_{xy}}{\partial x\,\partial y}+\frac{\partial^2 M_y}{\partial y^2}=I_0\left(\ddot{w}_b+\ddot{w}_s\right)+I_1\left(\frac{\partial \ddot{u}}{\partial x}+\frac{\partial \ddot{v}}{\partial y}\right)-I_2\nabla^2\ddot{w}_b-\nabla^2\left[L_0\left(\ddot{w}_b+\ddot{w}_s\right)+L_1\left(\frac{\partial \ddot{u}}{\partial x}+\frac{\partial \ddot{v}}{\partial y}\right)-L_2\nabla^2\ddot{w}_b\right],$$

$$\delta u_s\colon \frac{\partial Q_x}{\partial x}+\frac{\partial Q_y}{\partial y}=I_0\left(\ddot{w}_b+\ddot{w}_s\right)-\nabla^2\left[L_0\left(\ddot{w}_b+\ddot{w}_s\right)\right], \tag{16}$$

where N_i, M_i, L_i, and R_i are the local stress resultants which are calculated by

$$\begin{Bmatrix} N_x \\ N_y \\ N_{xy} \end{Bmatrix}=\int_{-h/2}^{h/2}\begin{Bmatrix} t_x \\ t_y \\ t_{xy} \end{Bmatrix}\mathrm{d}z,$$

$$\begin{Bmatrix} M_x \\ M_y \\ M_{xy} \end{Bmatrix}=\int_{-h/2}^{h/2}\begin{Bmatrix} t_x \\ t_y \\ t_{xy} \end{Bmatrix}z\mathrm{d}z, \tag{17}$$

$$\begin{Bmatrix} Q_x \\ Q_y \end{Bmatrix}=\int_{-h/2}^{h/2}\begin{Bmatrix} t_{xz} \\ t_{yz} \end{Bmatrix}\mathrm{d}z.$$

By substituting equations (11) and (12) into equation (17) and integrating through the thickness of the plates and then reordering these equations into matrix form, one gets

$$\begin{Bmatrix} \{N\} \\ \{M\} \\ \{Q\} \end{Bmatrix}=\begin{bmatrix} [A] & [B] & 0 \\ [B] & [D] & 0 \\ 0 & 0 & [H] \end{bmatrix}\begin{Bmatrix} \{\varepsilon^0\} \\ \{\kappa\} \\ \{\gamma^0\} \end{Bmatrix}, \tag{18}$$

where

$$\left(A_{ij}, B_{ij}, D_{ij}\right)=\int_{-h/2}^{h/2}C_{ij}\left(1, z, z^2\right)\mathrm{d}z,$$
$$\left(H_{ij}\right)=k_s\int_{-h/2}^{h/2}C_{ij}\mathrm{d}z, \tag{19}$$

where k_s being the shear correction factor, which is usually taken as $k_s = 5/6$. In the case of conventional nonlocal elasticity theory, the nonlocal parameter μ is assumed to be constant through the thickness of the plates and the coefficients I_0, I_1, I_2 and L_0, L_1, L_2 are calculated as the following formulas:

$$\left(I_0, I_1, I_2\right)=\int_{-h/2}^{h/2}\rho(z)\left(1, z, z^2\right)\mathrm{d}z, \tag{20}$$

$$\left(L_0, L_1, L_2\right)=\mu\int_{-h/2}^{h/2}\rho(z)\left(1, z, z^2\right)\mathrm{d}z. \tag{21}$$

When the nonlocal parameter μ is constant, one gets $(L_0, L_1, L_2) = \mu(I_0, I_1, I_2)$. Consequently, the governing equations of motion equation (16) become the conventional governing equations of motion of the nanoplates with the constant nonlocal parameter. In this study, the nonlocal parameter is assumed to vary through the thickness of the plates as other material properties. This is the novelty of the present study in comparison with other works. Such that the coefficients I_0, I_1, and I_2 are calculated via equation (20), while the coefficients L_0, L_1, and L_2 are calculated as follows:

$$\left(L_0, L_1, L_2\right)=\int_{-h/2}^{h/2}\mu(z)\rho(z)\left(1, z, z^2\right)\mathrm{d}z. \tag{22}$$

This is the novelty of the present study. The classical nonlocal elasticity theory with constant nonlocal parameter is achieved by setting $\mu_c/\mu_m = 1$; thus, $\mu_c = \mu_m = \mu$.

3.4. Analytical Solution. In this study, a fully simply supported nanoplate is considered. The simply supported edge is

$$\begin{aligned} N_x = v = w_b = w_s = M_x = 0, \quad &\text{at } x = 0, a, \\ u = N_y = w_b = w_s = M_y = 0, \quad &\text{at } y = 0, b. \end{aligned} \tag{23}$$

By applying Navier's solution, the displacement fields of the plates are assumed as

$$\begin{aligned} u(x, y, t) &= \sum_{m=1}^{\infty}\sum_{n=1}^{\infty}U_{mn}e^{i\omega t}\cos\alpha x\,\sin\beta y, \\ v(x, y, t) &= \sum_{m=1}^{\infty}\sum_{n=1}^{\infty}V_{mn}e^{i\omega t}\sin\alpha x\,\cos\beta y, \\ w_b(x, y, t) &= \sum_{m=1}^{\infty}\sum_{n=1}^{\infty}Wb_{mn}e^{i\omega t}\sin\alpha x\,\sin\beta y, \\ w_s(x, y, t) &= \sum_{m=1}^{\infty}\sum_{n=1}^{\infty}Ws_{mn}e^{i\omega t}\sin\alpha x\,\sin\beta y, \end{aligned} \tag{24}$$

where $\alpha = m\pi/a$, $\beta = n\pi/b$, $i^2 = -1$, $\Delta = \{U_{mn}, V_{mn}, Wb_{mn}, Ws_{mn}\}$, and ω is the free frequency of the nanoplates. Substituting equation (24) into equation (4) and then equation (16), one gets

$$\left(\mathbf{K}-\omega^2\mathbf{M}\right)\Delta=0, \tag{25}$$

where $\mathbf{K}$ and $\mathbf{M}$ are the stiffness matrix and the mass matrix and their elements are K_{ij} and M_{ij}, $i, j = \overline{1,4}$ which are calculated as the following formulas:

$$\begin{aligned}
K_{11} &= A_{11}\alpha^2 + A_{66}\beta^2;\\
K_{12} &= \alpha(A_{12} + A_{66})\beta;\\
K_{13} &= -B_{11}\alpha^3 - (B_{12} + 2B_{66})\beta^2\alpha;\\
K_{14} &= 0;\\
K_{22} &= A_{22}\beta^2 + A_{66}\alpha^2;\\
K_{23} &= -B_{22}\beta^3 - \alpha^2(B_{12} + 2B_{66})\beta;\\
K_{24} &= 0;\\
K_{33} &= D_{11}\alpha^4 + 2\beta^2(D_{12} + 2D_{66})\alpha^2 + D_{22}\beta^4;\\
K_{34} &= 0;\\
K_{44} &= H_{44}\beta^2 + H_{55}\alpha^2,\\
M_{11} &= (\alpha^2 + \beta^2)L_0 + I_0;\\
M_{12} &= 0;\\
M_{13} &= -\alpha((\alpha^2 + \beta^2)L_1 + I_1);\\
M_{14} &= 0;\\
M_{22} &= (\alpha^2 + \beta^2)L_0 + I_0;\\
M_{23} &= -\beta((\alpha^2 + \beta^2)L_1 + I_1);\\
M_{24} &= 0;\\
M_{33} &= L_2\alpha^4 + (2L_2\beta^2 + I_2 + L_0)\alpha^2 + L_2\beta^4 + (I_2 + L_0)\beta^2 + I_0;\\
M_{34} &= (\alpha^2 + \beta^2)L_0 + I_0;\\
M_{44} &= (\alpha^2 + \beta^2)L_0 + I_0.
\end{aligned} \tag{26}$$

4. Numerical Results and Discussion

4.1. Comparison Study. To present the validity of the current algorithm, the free vibration of fully simply supported square porous FGM plates is considered. The plates are made of Al/Al_2O_3, the dimensions of the plate are $a = b = 1$, and the thickness is h. The material properties of the perfect plates are calculated via power-law function, and the porosity is normally distributed through the thickness direction. Hence, the effective Young's modulus and effective mass density are computed as follows [55]:

$$\begin{aligned}
E(z) &= (E_c - E_m)\left(\frac{z}{h} + \frac{1}{2}\right)^k + E_m - (E_c + E_m)\frac{P_0}{2},\\
\rho(z) &= (\rho_c - \rho_m)\left(\frac{z}{h} + \frac{1}{2}\right)^k + \rho_m - (\rho_c + \rho_m)\frac{P_0}{2}.
\end{aligned} \tag{27}$$

The nondimensional frequencies of the plates are calculated as $\overline{\omega} = \omega h\sqrt{\rho_m/E_m}$. The present results are compared with those of Rezaei et al. [55] in Table 2. According to this table, it can be concluded that the proposed results are in good agreement with those of Rezaei et al. [55] using higher-order shear deformation theory (HSDT).

Secondly, the numerical results of free vibration of FGM nanoplates using the proposed theory are compared with those of Sobhy and Radwan [51]. In this subsection, the FGM nanoplates are made of $SUS304/Si_3N_4$ with several values of side-to-thickness ratio a/h, and nonlocal parameters μ are considered. The dimensions of the plates are $a = b = 10\,\text{nm}$ and the thickness is h. The effective material properties are calculated via a power-law function. The comparison between the nondimensional fundamental frequencies $\widehat{\omega} = 10\omega h\sqrt{\rho_m/E_m}$ of the FGM nanoplates of $SUS304/Si_3N_4$ using the present theory and those of Sobhy using simple HSDT and quasi-3D theory is shown in Table 3. According to this table, it can be concluded that the present results are in good agreement with those of Sobhy and Radwan [51].

4.2. Parameter Study. In the current investigation, a functionally graded nanoplate of Al/ZrO_2 with porosity is considered. The material properties of Al and ZrO_2 are given in Table 1. The nonlocal parameter of Al is assumed to be constant and given as $\mu_m = 2\,(\text{nm}^2)$ and plays as the reference nonlocal value. For convenience, the following nondimensional frequencies are used:

$$\Omega = 10\omega h\sqrt{\frac{\rho_m}{E_m}}. \tag{28}$$

Tables 4–8 show the nondimensional fundamental frequency of the FGM nanoplates with the dimension of $a = 10\,(\text{nm}^2)$ and the thickness of $h = a/10$. The nondimensional fundamental frequencies of four patterns of the porous FGM nanoplates are given in Tables 4–7. According to these tables, it can be seen that when the power-law index increases, the frequency of the FGM nanoplates decreases. Besides, the increase in the nonlocal parameter's ratio μ_c/μ_m leads to the decrease in the frequency of the FGM nanoplates. When the power-law index is infinity, $k = \infty$, the nondimensional fundamental frequency of the FGM nanoplates is independent of the variation of the nonlocal parameter's ratio. The reason is that when $k = \infty$, the FGM nanoplate becomes a fully metallic one; therefore, the nonlocal parameter is constant and equals the nonlocal parameter of the metal component through the thickness of the plate. Moreover, when the maximum porosity value P_0 increases, the nondimensional fundamental frequencies of the plates of type B and C decrease but those of the plates of types A and D increase because the increase in the maximum porosity coefficient P_0 leads to the decrease in both the stiffness and the mass of the plates. In the case of type A, most of the porosities are distributed around the middle plane of the plate, so the effect of the porosity to the mass matrix is stronger than that to the stiffness matrix. On the opposite side, the porosities of type B of the plate are distributed near two surfaces of the plate, so the effect of the porosity to the stiffness matrix is stronger than that to the mass matrix. In the case of type C, the porosity is distributed near the metal-rich surface, so the effect of the porosity to the stiffness is stronger than that to the mass. In the cases of type D, the porosity is distributed near the ceramic-rich surface, so the effect of the porosity on the mass is stronger than that to the stiffness.

Table 2: The comparison of the nondimensional frequencies of the FGM plates with porosity.

b/a	P_0	Method	$k = 0$	$k = 0.1$	$k = 0.5$	$k = 1$
$a/h = 5$						
0.5	0	Rezaei et al. [55]	0.271946	0.262017	0.231573	0.208997
		Present	0.270664	0.260810	0.230591	0.208158
	0.2	Rezaei et al. [55]	0.280478	0.268960	0.230875	0.198452
		Present	0.279155	0.267727	0.229933	0.197735
	0.4	Rezaei et al. [55]	0.292977	0.279294	0.228453	0.172779
		Present	0.291596	0.278020	0.227585	0.172308
1	0	Rezaei et al. [55]	0.418210	0.403221	0.357054	0.322491
		Present	0.415341	0.400515	0.354840	0.320598
	0.2	Rezaei et al. [55]	0.431330	0.413956	0.356290	0.306810
		Present	0.428371	0.411190	0.354161	0.305185
	0.4	Rezaei et al. [55]	0.450552	0.429936	0.353095	0.268252
		Present	0.447461	0.427079	0.351127	0.267173
$a/h = 10$						
0.5	0	Rezaei et al. [55]	0.071909	0.069208	0.060987	0.054979
		Present	0.071812	0.069118	0.060914	0.054916
	0.2	Rezaei et al. [55]	0.074165	0.071029	0.060721	0.052052
		Present	0.074065	0.070936	0.060651	0.051999
	0.4	Rezaei et al. [55]	0.077470	0.073737	0.059943	0.045029
		Present	0.077366	0.073641	0.059879	0.044995
1	0	Rezaei et al. [55]	0.113693	0.109449	0.096510	0.087024
		Present	0.113454	0.109225	0.096329	0.086869
	0.2	Rezaei et al. [55]	0.117260	0.112333	0.096119	0.082444
		Present	0.117013	0.112104	0.095945	0.082313
	0.4	Rezaei et al. [55]	0.122485	0.116624	0.094936	0.071421
		Present	0.122228	0.116387	0.094777	0.071336

Table 3: The comparison of the nondimensional frequencies of the FGM plates with porosity.

a/h	k	Method	$\mu = 0^2$	$\mu = 0.5^2$	$\mu = 1^2$	$\mu = 1.5^2$	$\mu = 2^2$
5	0	Sobhy and Radwan [51] (quais-3D)	5.12377	5.00184	4.68243	4.26370	3.83015
		Sobhy and Radwan [51] (HSDT)	5.10702	4.98549	4.66713	4.24976	3.81763
		Present	5.10587	4.98437	4.66607	4.24880	3.81677
	1	Sobhy and Radwan [51] (quais-3D)	3.04445	2.97200	2.78221	2.53340	2.27580
		Sobhy and Radwan [51] (HSDT)	3.01860	2.94677	2.75859	2.51190	2.25648
		Present	3.01873	2.94689	2.75871	2.51200	2.25657
	5	Sobhy and Radwan [51] (quais-3D)	2.44172	2.38362	2.23140	2.03185	1.82525
		Sobhy and Radwan [51] (HSDT)	2.42443	2.36674	2.21560	2.01747	1.81232
		Present	2.43356	2.37565	2.22395	2.02507	1.81915
	Metal	Sobhy and Radwan [51] (quais-3D)	2.12231	2.07180	1.93950	1.76606	1.58648
		Sobhy and Radwan [51] (HSDT)	2.11261	2.06234	1.93064	1.75799	1.57923
		Present	2.11208	2.06182	1.93015	1.75755	1.57883
10	0	Sobhy and Radwan [51] (quais-3D)	1.39015	1.35707	1.27041	1.15680	1.03917
		Sobhy and Radwan [51] (HSDT)	1.38829	1.35525	1.26871	1.15525	1.03778
		Present	1.38824	1.35521	1.26867	1.15521	1.03775
	1	Sobhy and Radwan [51] (quais-3D)	0.82782	0.80812	0.75652	0.68886	0.61882
		Sobhy and Radwan [51] (HSDT)	0.82250	0.80292	0.75165	0.68443	0.61484
		Present	0.82296	0.80338	0.75208	0.68482	0.61518
	5	Sobhy and Radwan [51] (quais-3D)	0.66890	0.65299	0.61129	0.55662	0.50002
		Sobhy and Radwan [51] (HSDT)	0.66485	0.64903	0.60758	0.55325	0.49699
		Present	0.66594	0.65009	0.60857	0.55415	0.49780
	Metal	Sobhy and Radwan [51] (quais-3D)	0.57817	0.56441	0.52837	0.48112	0.43220
		Sobhy and Radwan [51] (HSDT)	0.57695	0.56322	0.52725	0.48010	0.43128
		Present	0.57693	0.56320	0.52724	0.48009	0.43127

Table 3: Continued.

a/h	k	Method	$\mu = 0^2$	$\mu = 0.5^2$	$\mu = 1^2$	$\mu = 1.5^2$	$\mu = 2^2$
50	0	Sobhy and Radwan [51] (quais-3D)	0.05733	0.05596	0.05239	0.04770	0.04285
		Sobhy and Radwan [51] (HSDT)	0.05730	0.05593	0.05236	0.04768	0.04283
		Present	0.05730	0.05593	0.05236	0.04768	0.04283
	1	Sobhy and Radwan [51] (quais-3D)	0.03417	0.03335	0.03122	0.02843	0.02554
		Sobhy and Radwan [51] (HSDT)	0.03398	0.03317	0.03105	0.02827	0.02540
		Present	0.03401	0.03320	0.03108	0.02830	0.02542
	5	Sobhy and Radwan [51] (quais-3D)	0.02769	0.02703	0.02531	0.02304	0.02070
		Sobhy and Radwan [51] (HSDT)	0.02754	0.02688	0.02517	0.02291	0.02058
		Present	0.02756	0.02690	0.02518	0.02293	0.02060
	Metal	Sobhy and Radwan [51] (quais-3D)	0.02388	0.02331	0.02182	0.01987	0.01785
		Sobhy and Radwan [51] (HSDT)	0.02385	0.02329	0.02180	0.01985	0.01783
		Present	0.02386	0.02329	0.02180	0.01985	0.01784

Table 4: The nondimensional fundamental frequency of the porous FGM nanoplates of pattern A.

a/h	P_0	μ_c/μ_m	$k = 0$	$k = 0.5$	$k = 1$	$k = 2$	$k = 5$	$k = \infty$
5	0.1	0.5	1.1370	1.0503	1.0153	0.9978	0.9968	0.9044
		1	1.0535	0.9971	0.9745	0.9688	0.9803	0.9044
		1.5	0.9860	0.9512	0.9383	0.9421	0.9645	0.9044
		2	0.9301	0.9112	0.9058	0.9175	0.9495	0.9044
	0.2	0.5	1.1514	1.0630	1.0272	1.0095	1.0087	0.9158
		1	1.0668	1.0092	0.9859	0.9798	0.9915	0.9158
		1.5	0.9985	0.9628	0.9491	0.9525	0.9751	0.9158
		2	0.9418	0.9222	0.9162	0.9274	0.9595	0.9158
	0.5	0.5	1.2070	1.1119	1.0731	1.0541	1.0536	0.9600
		1	1.1183	1.0557	1.0294	1.0216	1.0335	0.9600
		1.5	1.0467	1.0073	0.9906	0.9920	1.0146	0.9600
		2	0.9873	0.9650	0.9559	0.9648	0.9966	0.9600
10	0.1	0.5	0.6225	0.5724	0.5530	0.5452	0.5489	0.4951
		1	0.5768	0.5433	0.5307	0.5293	0.5398	0.4951
		1.5	0.5398	0.5182	0.5108	0.5146	0.5311	0.4951
		2	0.5092	0.4963	0.4931	0.5011	0.5229	0.4951
	0.2	0.5	0.6319	0.5806	0.5607	0.5528	0.5566	0.5026
		1	0.5855	0.5510	0.5380	0.5364	0.5471	0.5026
		1.5	0.5480	0.5256	0.5178	0.5214	0.5381	0.5026
		2	0.5169	0.5034	0.4998	0.5076	0.5295	0.5026
	0.5	0.5	0.6688	0.6127	0.5907	0.5819	0.5862	0.5319
		1	0.6196	0.5816	0.5665	0.5638	0.5750	0.5319
		1.5	0.5800	0.5548	0.5449	0.5473	0.5644	0.5319
		2	0.5470	0.5314	0.5257	0.5322	0.5544	0.5319

Continuously, the influence of the porosity on the fundamental frequency of the square FGM nanoplate is considered. The nondimensional fundamental frequency of perfect FGM nanoplates is given in Table 8. In the cases of $a/h = 10$ and $\mu_c/\mu_m = 2$, Figure 3 presents the variation of the nondimensional fundamental frequency of the FGM nanoplates as functions of maximum porosity value P_0. It can be seen that the effects of the porosity on four types of porosity dispersion are different. When $P_0 = 0$, the fundamental frequencies of the FGM nanoplates of four patterns A, B, C, and D are identical because these porous FGM nanoplates become perfect ones. For pattern A, when P_0 increases, the fundamental frequency increases rapidly for both $k = 0.5$ and $k = 2$. On the opposite side, when P_0 increases, the fundamental frequency of pattern B decreases rapidly for both $k = 0.5$ and $k = 2$. The fundamental frequency for pattern C decreases slower than that of pattern B, and the fundamental frequency of pattern D increases slower than that of pattern A.

To investigate the effects of the porosity on the high frequencies of the square FGM nanoplates, the frequencies of four modes (5, 5), (10, 10), (20, 20), and (100, 100) are considered. Figure 4 presents the ratio between the frequencies of the FGM nanoplates with porosity and those of the perfect FGM nanoplates $\Omega_{m,n}^{\text{porous}}/\Omega_{m,n}^{\text{perfect}}$. It can be seen clearly that the effects of the porosity on the high frequencies are different from those on the low frequencies. For mode (5, 5), the effects of the porosity of patterns A and B are stronger than those of patterns C and D. For mode (10, 10), the strong effects of porosity of four patterns are similar with two different trends and the frequencies of patterns A and D increase while those of patterns B and C decrease. For mode (20, 20), the influences of the porosity of patterns C and D on the

Table 5: The nondimensional fundamental frequency of the porous FGM nanoplates of pattern B.

a/h	P_0	μ_c/μ_m	$k = 0$	$k = 0.5$	$k = 1$	$k = 2$	$k = 5$	$k = \infty$
5	0.1	0.5	1.1114	1.0277	0.9938	0.9767	0.9753	0.8840
		1	1.0297	0.9756	0.9541	0.9488	0.9600	0.8840
		1.5	0.9638	0.9307	0.9188	0.9232	0.9453	0.8840
		2	0.9091	0.8914	0.8872	0.8996	0.9313	0.8840
	0.2	0.5	1.0973	1.0153	0.9820	0.9650	0.9633	0.8728
		1	1.0167	0.9637	0.9428	0.9377	0.9486	0.8728
		1.5	0.9515	0.9194	0.9081	0.9127	0.9345	0.8728
		2	0.8975	0.8806	0.8769	0.8895	0.9211	0.8728
	0.5	0.5	1.0442	0.9686	0.9371	0.9203	0.9172	0.8306
		1	0.9675	0.9193	0.9002	0.8953	0.9048	0.8306
		1.5	0.9056	0.8769	0.8673	0.8723	0.8928	0.8306
		2	0.8542	0.8399	0.8377	0.8510	0.8813	0.8306
10	0.1	0.5	0.6059	0.5579	0.5393	0.5318	0.5350	0.4819
		1	0.5614	0.5295	0.5177	0.5165	0.5266	0.4819
		1.5	0.5254	0.5050	0.4984	0.5025	0.5186	0.4819
		2	0.4956	0.4837	0.4812	0.4895	0.5109	0.4819
	0.2	0.5	0.5969	0.5500	0.5318	0.5243	0.5273	0.4747
		1	0.5530	0.5220	0.5105	0.5094	0.5193	0.4747
		1.5	0.5176	0.4979	0.4916	0.4957	0.5116	0.4747
		2	0.4882	0.4768	0.4746	0.4831	0.5043	0.4747
	0.5	0.5	0.5634	0.5207	0.5038	0.4963	0.4981	0.4481
		1	0.5220	0.4942	0.4838	0.4828	0.4914	0.4481
		1.5	0.4886	0.4713	0.4661	0.4703	0.4849	0.4481
		2	0.4608	0.4514	0.4502	0.4588	0.4787	0.4481

Table 6: The nondimensional fundamental frequency of the porous FGM nanoplates of pattern C.

a/h	P_0	μ_c/μ_m	$k = 0$	$k = 0.5$	$k = 1$	$k = 2$	$k = 5$	$k = \infty$
5	0.1	0.5	1.1263	1.0394	1.0039	0.9859	0.9854	0.8959
		1	1.0436	0.9862	0.9631	0.9567	0.9688	0.8959
		1.5	0.9768	0.9404	0.9269	0.9300	0.9531	0.8959
		2	0.9213	0.9005	0.8944	0.9055	0.9381	0.8959
	0.2	0.5	1.1277	1.0388	1.0022	0.9832	0.9834	0.8970
		1	1.0449	0.9850	0.9607	0.9534	0.9662	0.8970
		1.5	0.9780	0.9389	0.9240	0.9261	0.9499	0.8970
		2	0.9224	0.8986	0.8911	0.9010	0.9343	0.8970
	0.5	0.5	1.1206	1.0249	0.9845	0.9616	0.9635	0.8913
		1	1.0383	0.9696	0.9408	0.9293	0.9440	0.8913
		1.5	0.9718	0.9224	0.9025	0.9000	0.9256	0.8913
		2	0.9166	0.8815	0.8685	0.8733	0.9082	0.8913
10	0.1	0.5	0.6156	0.5652	0.5456	0.5374	0.5413	0.4896
		1	0.5703	0.5362	0.5233	0.5214	0.5322	0.4896
		1.5	0.5338	0.5112	0.5035	0.5068	0.5235	0.4896
		2	0.5035	0.4894	0.4858	0.4933	0.5153	0.4896
	0.2	0.5	0.6164	0.5648	0.5444	0.5355	0.5398	0.4903
		1	0.5712	0.5354	0.5217	0.5191	0.5303	0.4903
		1.5	0.5346	0.5102	0.5016	0.5042	0.5213	0.4903
		2	0.5042	0.4883	0.4837	0.4904	0.5128	0.4903
	0.5	0.5	0.6119	0.5556	0.5326	0.5211	0.5261	0.4867
		1	0.5669	0.5254	0.5088	0.5033	0.5153	0.4867
		1.5	0.5306	0.4997	0.4879	0.4873	0.5052	0.4867
		2	0.5005	0.4775	0.4694	0.4728	0.4956	0.4867

frequencies of porous FGM nanoplates are stronger than those of patterns A and B. For mode (100, 100), the porosity of patterns C and D affects strongly the free vibration of porous FGM nanoplates but the frequencies of the FGM nanoplates of patterns A and B are almost unchanged.

The role of the variable nonlocal parameter on the free vibration of the square porous FGM nanoplates with $a/h = 10$ is investigated and presented in Figure 5. Generally, the fundamental frequency of the nanoplates decreases with the increase in the nonlocal parameter ratio μ_c/μ_m; however, the effects of the nonlocal parameters are different from

Table 7: The nondimensional fundamental frequency of the porous FGM nanoplates of pattern D.

a/h	P_0	μ_c/μ_m	$k = 0$	$k = 0.5$	$k = 1$	$k = 2$	$k = 5$	$k = \infty$
5	0.1	0.5	1.1263	1.0424	1.0088	0.9922	0.9904	0.8959
		1	1.0436	0.9901	0.9690	0.9642	0.9748	0.8959
		1.5	0.9768	0.9449	0.9336	0.9385	0.9600	0.8959
		2	0.9213	0.9054	0.9018	0.9147	0.9458	0.8959
	0.2	0.5	1.1277	1.0454	1.0128	0.9970	0.9943	0.8970
		1	1.0449	0.9936	0.9735	0.9696	0.9792	0.8970
		1.5	0.9780	0.9487	0.9385	0.9443	0.9648	0.8970
		2	0.9224	0.9094	0.9071	0.9209	0.9510	0.8970
	0.5	0.5	1.1206	1.0471	1.0190	1.0063	0.9992	0.8913
		1	1.0383	0.9977	0.9826	0.9817	0.9863	0.8913
		1.5	0.9718	0.9547	0.9498	0.9588	0.9738	0.8913
		2	0.9166	0.9168	0.9201	0.9375	0.9619	0.8913
10	0.1	0.5	0.6156	0.5674	0.5490	0.5418	0.5449	0.4896
		1	0.5703	0.5388	0.5272	0.5265	0.5364	0.4896
		1.5	0.5338	0.5142	0.5079	0.5123	0.5282	0.4896
		2	0.5035	0.4926	0.4905	0.4993	0.5205	0.4896
	0.2	0.5	0.6164	0.5694	0.5517	0.5451	0.5477	0.4903
		1	0.5712	0.5411	0.5302	0.5301	0.5394	0.4903
		1.5	0.5346	0.5166	0.5111	0.5162	0.5315	0.4903
		2	0.5042	0.4952	0.4939	0.5034	0.5240	0.4903
	0.5	0.5	0.6119	0.5710	0.5564	0.5520	0.5517	0.4867
		1	0.5669	0.5440	0.5365	0.5385	0.5446	0.4867
		1.5	0.5306	0.5205	0.5186	0.5260	0.5379	0.4867
		2	0.5005	0.4998	0.5023	0.5143	0.5314	0.4867

Table 8: The nondimensional fundamental frequency of the perfect FGM nanoplates.

a/h	P_0	μ_c/μ_m	$k = 0$	$k = 0.5$	$k = 1$	$k = 2$	$k = 5$	$k = \infty$
5	0	0.5	1.1242	1.0390	1.0045	0.9873	0.9861	0.8942
		1	1.0416	0.9863	0.9643	0.9588	0.9701	0.8942
		1.5	0.9749	0.9409	0.9286	0.9327	0.9550	0.8942
		2	0.9196	0.9013	0.8965	0.9086	0.9405	0.8942
10	0	0.5	0.6142	0.5651	0.5461	0.5385	0.5419	0.4885
		1	0.5690	0.5363	0.5241	0.5229	0.5332	0.4885
		1.5	0.5326	0.5116	0.5046	0.5085	0.5249	0.4885
		2	0.5024	0.4899	0.4871	0.4953	0.5169	0.4885

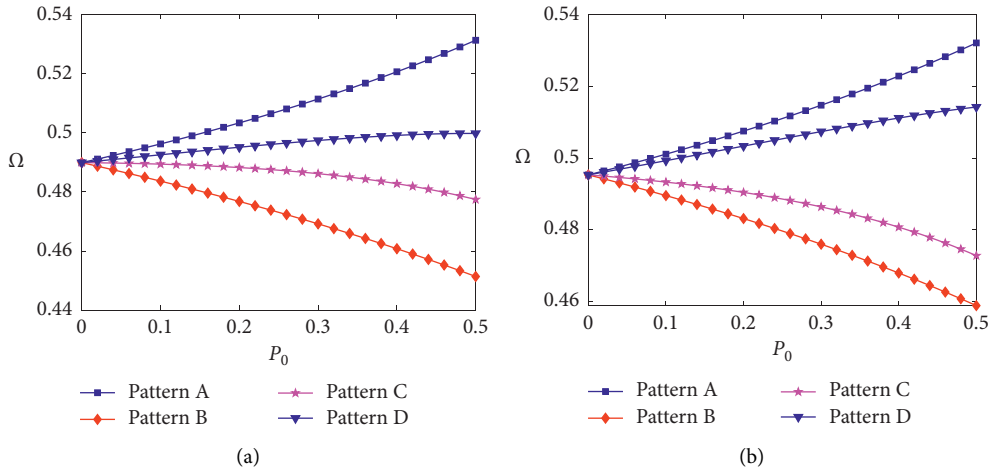

Figure 3: The effects of porosity on the fundamental frequencies of the porous FGM nanoplates: (a) $\mu_c/\mu_m = 2$ and $k = 0.5$; (b) $\mu_c/\mu_m = 2$ and $k = 2$.

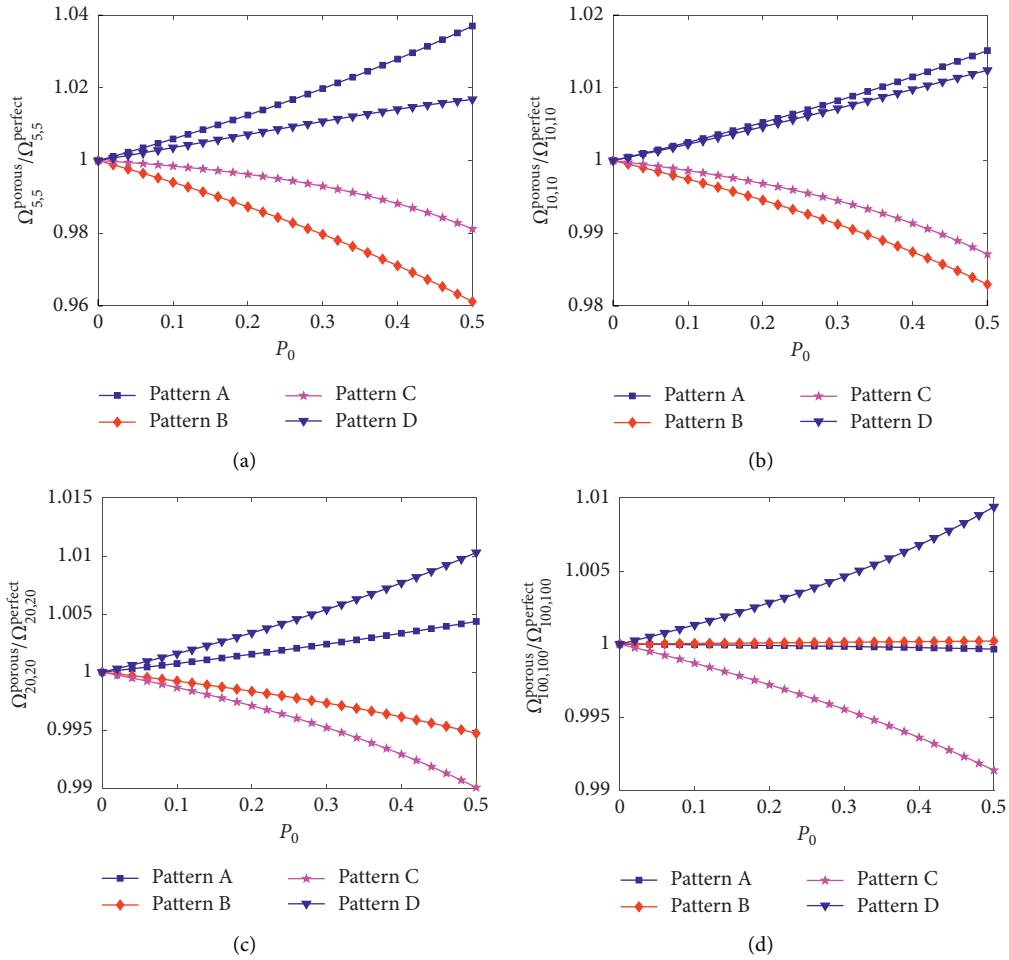

FIGURE 4: The effects of porosity on the high frequencies of the porous FGM nanoplates: (a) Mode (5, 5); (b) Mode (10, 10); (c) Mode (20, 20); (d) Mode (100, 100).

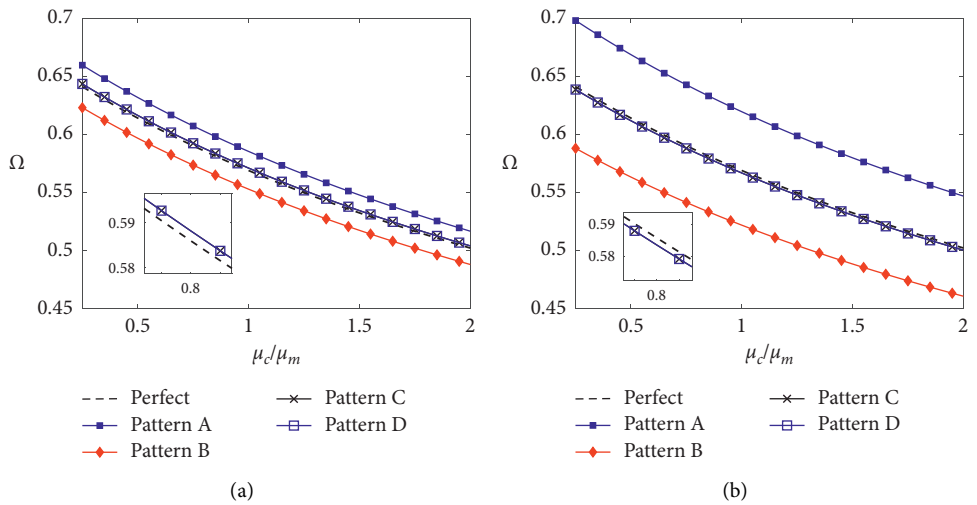

FIGURE 5: Continued.

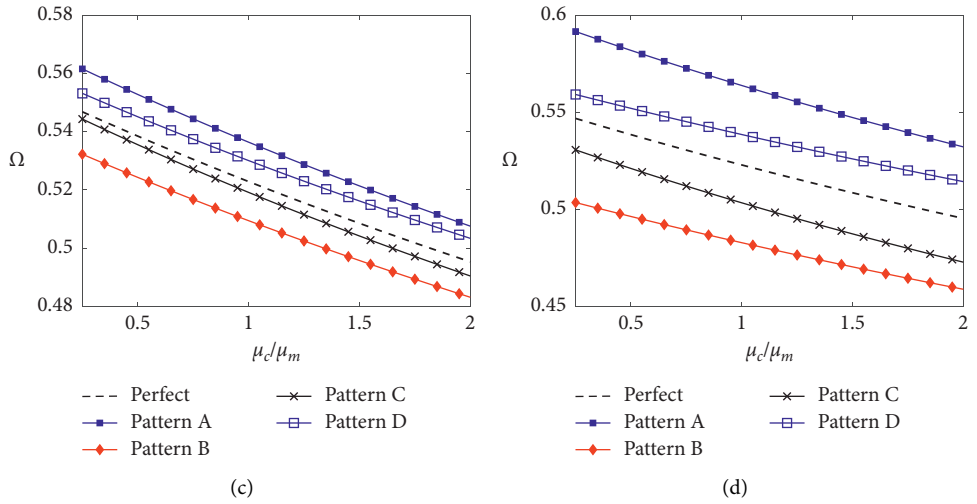

FIGURE 5: The effects of the variation of the nonlocal parameter on fundamental frequencies of the porous FGM nanoplates: (a) $k = 0$ and $P_0 = 0.2$; (b) $k = 0$ and $P_0 = 0.5$; (c) $k = 2$ and $P_0 = 0.2$; (d) $k = 2$ and $P_0 = 0.5$.

homogeneous perfect nanoplates. Figures 5(a) and 5(b) demonstrate the effects of the increase in the nonlocal parameters ratio on the nondimensional fundamental frequencies of the homogeneous nanoplates ($k = 0$). It can be seen that the effects of the nonlocal parameters ratio on the fundamental frequencies of the nanoplates depend on the patterns and coefficients of porosity. Besides, the effects of the porosity of patterns A and B are significant than those of patterns C and D of porosity. In the cases of FGM nanoplates with $k = 2$, the effects of the nonlocal parameters ratio μ_c/μ_m on the nondimensional fundamental frequencies of the FGM nanoplates are more different from those of the homogeneous ones as shown in Figures 5(c) and 5(d). When the porosity parameters are small $P_0 = 0.2$, the fundamental frequencies of the FGM nanoplates decrease at similar rate with the increase in the nonlocal parameters ratio μ_c/μ_m. When $P_0 = 0.5$ and $k = 2$, the decrease rates of the FGM porous nanoplates of patterns A and B are similar to the perfect ones. The rate of reduction of the fundamental frequencies of the FGM porous nanoplates of pattern C is higher than the perfect ones, while the rate of reduction of the fundamental frequencies of the FGM porous nanoplates of pattern D is slower than the perfect ones. Therefore, the effects of the nonlocal parameters ratio on the fundamental frequencies of the FGM porous nanoplates depend on power-law index k, porosity parameter P_0, and the distribution of porosity.

Figure 6 demonstrates the influence of the power-law index on the nondimensional fundamental frequencies of the square FGM nanoplates with porosity and $a/h = 10$ and $P_0 = 0.5$. When $\mu_c/\mu_m = 0.5$, the fundamental frequency of the porous FGM nanoplates decreases rapidly when the power-law index k increases from 0 to 2. When $k > 2$, the fundamental frequencies of the porous FGM nanoplates of patterns A and C increase slowly. For patterns B and D, the fundamental frequencies increase slowly when the power-law index k increases from 2 to 4, and the fundamental frequencies decrease gently when $k > 4$. When $\mu_c/\mu_m = 2$, the fundamental frequencies of four patterns decrease with the increase in the power-law index from 0 to 1. When $k > 1$, the fundamental frequencies increase with the increase in the power-law index. Especially, a minimum frequency exists when the power-law index increases. In the practical application, this phenomenon should be noticed to avoid the resonance behavior of the nanoplates. Besides, when the power-law index is equal to zero $k = 0$, the fundamental frequencies of patterns C and D are similar. The reason is that when $k = 0$, the FGM porous nanoplates become the homogeneous isotropic ones, so the effects of the porosity of patterns C and D are similar.

The influences of the porosity on the fundamental frequencies of the rectangular porous FGM nanoplates with $a/h = 10$ and $k = 2$ are investigated in this subsection. According to Figure 7, the fundamental frequencies of the porous FGM nanoplates decrease when the aspect ratio of b/a increases. In general, the frequencies of the FGM nanoplates with the aspect ratio of $b/a = 5$ are two times smaller than those of square ones, and the frequencies of the square ones are the highest. When the aspect ratio increases from 1 to 2, the fundamental frequency of the FGM porous nanoplates decreases dramatically. When the aspect ratio greater than 2, the fundamental frequency of the FGM porous nanoplates decrease slowly.

Lastly, the dependence of the fundamental frequencies of the square FGM porous nanoplates with $k = 2$ on the variation of the side-to-thickness ratio a/h is examined. Figure 8 shows that the fundamental frequencies of the square FGM nanoplates with decrease in porosity rapidly as the side-to-thickness ratio increases. The fundamental frequencies of the square porous FGM nanoplates with $a/h = 20$ are approximately five times smaller than those of the plates with $a/h = 5$. The fundamental frequencies of the square porous FGM nanoplates are increasing in order of pattern B, C, D, and A.

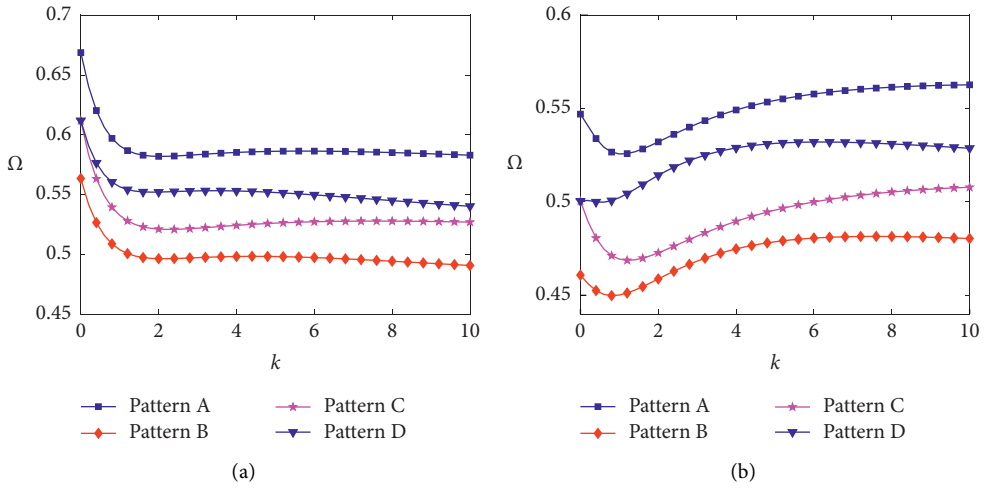

Figure 6: The influence of the power-law index on the fundamental frequencies of the porous FGM nanoplates: (a) $\mu_c/\mu_m = 0.5$ and $P_0 = 0.5$; (b) $\mu_c/\mu_m = 2$ and $P_0 = 0.5$.

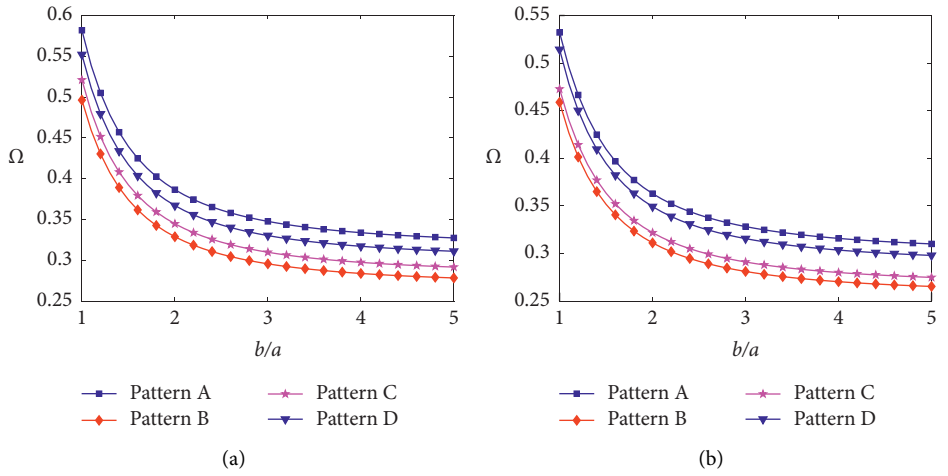

Figure 7: The effects of the aspect ratio on the fundamental frequencies of the FGM nanoplates: (a) $\mu_c/\mu_m = 0.5$ and $P_0 = 0.5$; (b) $\mu_c/\mu_m = 2$ and $P_0 = 0.5$.

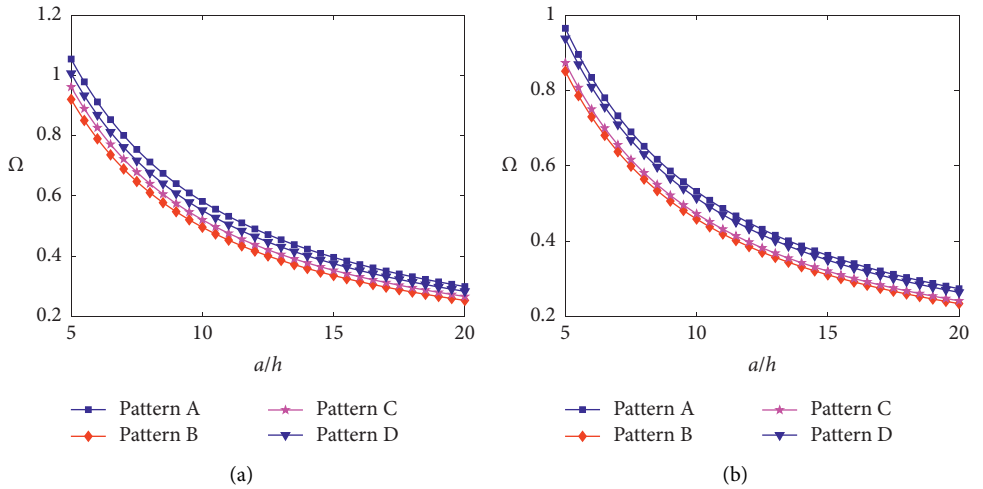

Figure 8: The influence of the side-to-thickness ratio on the fundamental frequencies of the porous FGM nanoplates: (a) $\mu_c/\mu_m = 0.5$ and $P_0 = 0.5$; (b) $\mu_c/\mu_m = 2$ and $P_0 = 0.5$.

5. Conclusions

A comprehensive study on the effects of porosity and variable nonlocal parameter on the free vibration of the porous FGM nanoplates has been presented. A modified nonlocal elasticity theory with the variation of the nonlocal parameter has been established to analyze the nonlocal free vibration of FGM nanoplates. The numerical results presented the significant effects of the porosity and variable nonlocal parameter on the free vibration behavior of the FGM nanoplates. Depending on the dispersion and coefficient of the porosity, the frequencies of the nanoplates can increase or decrease. Several remarkable conclusions can be read as follows:

(i) The variation of the nonlocal parameter should be considered due to its important role in the free vibration of FGM nanoplates

(ii) The inclusion of the nonlocal parameter leads to the decrease in the frequency of the nonlocal porous FGM plates

(iii) The porosity plays significant effects on the free vibration characteristics of the porous FGM nanoplates

(iv) The influence of the porosity on the high frequencies is different from that of the low frequencies of the FGM nanoplates

The outcomes of this study can serve as benchmark results for future works on the vibration analysis of micro/nanostructures considering the variable of small-scale parameters as well as the effects of the porosity.

Data Availability

No data were used to support this study.

Conflicts of Interest

On behalf of all authors, the corresponding author states that there are no conflicts of interest.

References

[1] F. Yang, A. C. M. Chong, D. C. C. Lam, and P. Tong, "Couple stress based strain gradient theory for elasticity," *International Journal of Solids and Structures*, vol. 39, no. 10, pp. 2731–2743, 2002.

[2] S. K. Park and X.-L. Gao, "Bernoulli-Euler beam model based on a modified couple stress theory," *Journal of Micromechanics and Microengineering*, vol. 16, no. 11, pp. 2355–2359, 2006.

[3] H. Ma, X. Gao, and J. Reddy, "A microstructure-dependent Timoshenko beam model based on a modified couple stress theory," *Journal of the Mechanics and Physics of Solids*, vol. 56, no. 12, pp. 3379–3391, 2008.

[4] M. Asghari, M. H. Kahrobaiyan, and M. T. Ahmadian, "A nonlinear Timoshenko beam formulation based on the modified couple stress theory," *International Journal of Engineering Science*, vol. 48, no. 12, pp. 1749–1761, 2010.

[5] A. C. Eringen, "Nonlocal polar elastic continua," *International Journal of Engineering Science*, vol. 10, no. 1, pp. 1–16, 1972.

[6] A. C. Eringen and D. G. B. Edelen, "On nonlocal elasticity," *International Journal of Engineering Science*, vol. 10, no. 3, pp. 233–248, 1972.

[7] A. C. Eringen, "On differential equations of nonlocal elasticity and solutions of screw dislocation and surface waves," *Journal of Applied Physics*, vol. 54, no. 9, pp. 4703–4710, 1983.

[8] N. A. Fleck, G. M. Muller, M. F. Ashby, and J. W. Hutchinson, "Strain gradient plasticity: theory and experiment," *Acta Metallurgica et Materialia*, vol. 42, no. 2, pp. 475–487, 1994.

[9] H. Sadeghi, M. Baghani, and R. Naghdabadi, "Strain gradient elasticity solution for functionally graded micro-cylinders," *International Journal of Engineering Science*, vol. 50, no. 1, pp. 22–30, 2012.

[10] C. W. Lim, G. Zhang, and J. N. Reddy, "A higher-order nonlocal elasticity and strain gradient theory and its applications in wave propagation," *Journal of the Mechanics and Physics of Solids*, vol. 78, pp. 298–313, 2015.

[11] F. Ebrahimi, M. R. Barati, and A. Dabbagh, "A nonlocal strain gradient theory for wave propagation analysis in temperature-dependent inhomogeneous nanoplates," *International Journal of Engineering Science*, vol. 107, pp. 169–182, 2016.

[12] M. R. Barati, "A general nonlocal stress-strain gradient theory for forced vibration analysis of heterogeneous porous nanoplates," *European Journal of Mechanics - A: Solids*, vol. 67, pp. 215–230, 2018.

[13] M. N. M. Allam and A. F. Radwan, "Nonlocal strain gradient theory for bending, buckling, and vibration of viscoelastic functionally graded curved nanobeam embedded in an elastic medium," *Advances in Mechanical Engineering*, vol. 11, Article ID 1687814019837067, 2019.

[14] H.-T. Thai, T. P. Vo, T.-K. Nguyen, and S.-E. Kim, "A review of continuum mechanics models for size-dependent analysis of beams and plates," *Composite Structures*, vol. 177, pp. 196–219, 2017.

[15] Y. Q. Zhang, G. R. Liu, and J. S. Wang, "Small-scale effects on buckling of multiwalled carbon nanotubes under axial compression," *Physical Review B*, vol. 70, no. 20, Article ID 205430, 2004.

[16] Y. Hu, K. Liew, Q. Wang, X. He, and B. Yakobson, "Nonlocal shell model for elastic wave propagation in single- and double-walled carbon nanotubes," *Journal of the Mechanics and Physics of Solids*, vol. 56, no. 12, pp. 3475–3485, 2008.

[17] R. Li and G. A. Kardomateas, "Vibration characteristics of multiwalled carbon nanotubes embedded in elastic media by a nonlocal elastic shell model," *Journal of Applied Mechanics*, vol. 74, no. 6, pp. 1087–1094, 2007.

[18] Q. Wang and V. K. Varadan, "Application of nonlocal elastic shell theory in wave propagation analysis of carbon nanotubes," *Smart Materials and Structures*, vol. 16, no. 1, pp. 178–190, 2007.

[19] H. Rouhi and R. Ansari, "Nonlocal analytical Flugge shell model for axial buckling of double-walled carbon nanotubes with different end conditions," *Nano*, vol. 07, no. 03, Article ID 1250018, 2012.

[20] S. C. Pradhan and J. K. Phadikar, "Small scale effect on vibration of embedded multilayered graphene sheets based on nonlocal continuum models," *Physics Letters A*, vol. 373, no. 11, pp. 1062–1069, 2009.

[21] T. Aksencer and M. Aydogdu, "Levy type solution method for vibration and buckling of nanoplates using nonlocal elasticity

theory," *Physica E: Low-Dimensional Systems and Nanostructures*, vol. 43, no. 4, pp. 954–959, 2011.

[22] Z.-B. Shen, H.-L. Tang, D.-K. Li, and G.-J. Tang, "Vibration of single-layered graphene sheet-based nanomechanical sensor via nonlocal Kirchhoff plate theory," *Computational Materials Science*, vol. 61, pp. 200–205, 2012.

[23] Y. Zhang, Z. X. Lei, L. W. Zhang, K. M. Liew, and J. L. Yu, "Nonlocal continuum model for vibration of single-layered graphene sheets based on the element-free kp-Ritz method," *Engineering Analysis with Boundary Elements*, vol. 56, pp. 90–97, 2015.

[24] Y. Zhang, L. W. Zhang, K. M. Liew, and J. L. Yu, "Buckling analysis of graphene sheets embedded in an elastic medium based on the kp-Ritz method and non-local elasticity theory," *Engineering Analysis with Boundary Elements*, vol. 70, pp. 31–39, 2016.

[25] R. Ansari, S. Sahmani, and B. Arash, "Nonlocal plate model for free vibrations of single-layered graphene sheets," *Physics Letters A*, vol. 375, no. 1, pp. 53–62, 2010.

[26] R. Ansari, B. Arash, and H. Rouhi, "Vibration characteristics of embedded multi-layered graphene sheets with different boundary conditions via nonlocal elasticity," *Composite Structures*, vol. 93, no. 9, pp. 2419–2429, 2011.

[27] S. Hosseini-Hashemi, M. Bedroud, and R. Nazemnezhad, "An exact analytical solution for free vibration of functionally graded circular/annular Mindlin nanoplates via nonlocal elasticity," *Composite Structures*, vol. 103, pp. 108–118, 2013.

[28] A. Anjomshoa and M. Tahani, "Vibration analysis of orthotropic circular and elliptical nano-plates embedded in elastic medium based on nonlocal Mindlin plate theory and using Galerkin method," *Journal of Mechanical Science and Technology*, vol. 30, no. 6, pp. 2463–2474, 2016.

[29] B. Fatima, B. K. Halim, B. Ismahene, and T. Abdelouahed, "A nonlocal zeroth-order shear deformation theory for free vibration of functionally graded nanoscale plates resting on elastic foundation," *Steel and Composite Structures*, vol. 20, pp. 227–249, 2016.

[30] A. M. Zenkour, "Nonlocal elasticity and shear deformation effects on thermal buckling of a CNT embedded in a viscoelastic medium," *The European Physical Journal Plus*, vol. 133, no. 5, p. 196, 2018.

[31] A. M. Zenkour and A. F. Radwan, "Nonlocal mixed variational formula for orthotropic nanoplates resting on elastic foundations," *The European Physical Journal Plus*, vol. 135, no. 6, p. 493, 2020.

[32] A. M. Zenkour, Z. S. Hafed, and A. F. Radwan, "Bending analysis of functionally graded nanoscale plates by using nonlocal mixed variational formula," *Mathematics*, vol. 8, 2020.

[33] R. Aghababaei and J. N. Reddy, "Nonlocal third-order shear deformation plate theory with application to bending and vibration of plates," *Journal of Sound and Vibration*, vol. 326, no. 1-2, pp. 277–289, 2009.

[34] R. Ansari and S. Sahmani, "Prediction of biaxial buckling behavior of single-layered graphene sheets based on nonlocal plate models and molecular dynamics simulations," *Applied Mathematical Modelling*, vol. 37, no. 12-13, pp. 7338–7351, 2013.

[35] S. Hosseini-Hashemi, M. Kermajani, and R. Nazemnezhad, "An analytical study on the buckling and free vibration of rectangular nanoplates using nonlocal third-order shear deformation plate theory," *European Journal of Mechanics - A: Solids*, vol. 51, pp. 29–43, 2015.

[36] A. Daneshmehr, A. Rajabpoor, and M. Pourdavood, "Stability of size dependent functionally graded nanoplate based on nonlocal elasticity and higher order plate theories and different boundary conditions," *International Journal of Engineering Science*, vol. 82, pp. 84–100, 2014.

[37] A. Daneshmehr, A. Rajabpoor, and A. Hadi, "Size dependent free vibration analysis of nanoplates made of functionally graded materials based on nonlocal elasticity theory with high order theories," *International Journal of Engineering Science*, vol. 95, pp. 23–35, 2015.

[38] P. Malekzadeh and M. Shojaee, "Free vibration of nanoplates based on a nonlocal two-variable refined plate theory," *Composite Structures*, vol. 95, pp. 443–452, 2013.

[39] S. Narendar, "Buckling analysis of micro-/nano-scale plates based on two-variable refined plate theory incorporating nonlocal scale effects," *Composite Structures*, vol. 93, no. 12, pp. 3093–3103, 2011.

[40] S. Narendar and S. Gopalakrishnan, "Scale effects on buckling analysis of orthotropic nanoplates based on nonlocal two-variable refined plate theory," *Acta Mechanica*, vol. 223, no. 2, pp. 395–413, 2012.

[41] L. K. Hoa, P. Van Vinh, N. D. Duc, N. T. Trung, L. T. Son, and D. Van Thom, "Bending and free vibration analyses of functionally graded material nanoplates via a novel nonlocal single variable shear deformation plate theory," *Proceedings - Institution of Mechanical Engineers Part C J. Mech. Eng. Sci.*, 2020.

[42] M. Sobhy, "Generalized two-variable plate theory for multi-layered graphene sheets with arbitrary boundary conditions," *Acta Mechanica*, vol. 225, no. 9, pp. 2521–2538, 2014.

[43] M. Sobhy, "Levy-type solution for bending of single-layered graphene sheets in thermal environment using the two-variable plate theory," *International Journal of Mechanical Sciences*, vol. 90, pp. 171–178, 2015.

[44] M. Sobhy, "Hygrothermal deformation of orthotropic nanoplates based on the state-space concept," *Composites Part B: Engineering*, vol. 79, pp. 224–235, 2015.

[45] M. Sobhy, "Hygrothermal vibration of orthotropic double-layered graphene sheets embedded in an elastic medium using the two-variable plate theory," *Applied Mathematical Modelling*, vol. 40, no. 1, pp. 85–99, 2016.

[46] M. Sobhy and A. M. Zenkour, "Nonlocal thermal and mechanical buckling of nonlinear orthotropic viscoelastic nanoplates embedded in a visco-pasternak medium," *International Journal of Applied Mechanics*, vol. 10, no. 08, Article ID 1850086, 2018.

[47] A. M. Zenkour and M. Sobhy, "Nonlocal elasticity theory for thermal buckling of nanoplates lying on Winkler-Pasternak elastic substrate medium," *Physica E: Low-Dimensional Systems and Nanostructures*, vol. 53, pp. 251–259, 2013.

[48] H.-T. Thai, T. P. Vo, T.-K. Nguyen, and J. Lee, "A nonlocal sinusoidal plate model for micro/nanoscale plates," *Proceedings of the Institution of Mechanical Engineers - Part C: Journal of Mechanical Engineering Science*, vol. 228, no. 14, pp. 2652–2660, 2014.

[49] A. M. Fattahi, B. Safaei, and E. Moaddab, "The application of nonlocal elasticity to determine vibrational behavior of FG nanoplates, steel," *Composite Structures*, vol. 32, no. 2, pp. 281–292, 2019.

[50] S. Sahmani and B. Safaei, "Large-amplitude oscillations of composite conical nanoshells with in-plane heterogeneity including surface stress effect," *Applied Mathematical Modelling*, vol. 89, pp. 1792–1813, 2021.

[51] M. Sobhy and A. F. Radwan, "A new quasi 3D nonlocal plate theory for vibration and buckling of FGM nanoplates," *International Journal of Applied Mechanics*, vol. 09, no. 01, Article ID 1750008, 2017.

[52] A. Bessaim, M. S. A. Houari, F. Bernard, and A. Tounsi, "A nonlocal quasi-3D trigonometric plate model for free vibration behaviour of micro/nanoscale plates," *Structural Engineering & Mechanics*, vol. 56, no. 2, pp. 223–240, 2015.

[53] V. T Do, P. V. Vinh, and H. N. Nguyen, "On the development of refined plate theory for static bending behavior of functionally graded plates," *Mathematical Problems in Engineering*, vol. 2020, Article ID 2836763, 13 pages, 2020.

[54] P. V. Vinh, "Formulation of a new mixed four-node quadrilateral element for static bending analysis of variable thickness functionally graded material plates," *Mathematical Problems in Engineering*, vol. 2021, Article ID 6653350, 23 pages, 2021.

[55] A. S. Rezaei, A. R. Saidi, M. Abrishamdari, and M. H. P. Mohammadi, "Natural frequencies of functionally graded plates with porosities via a simple four variable plate theory: an analytical approach," *Thin-Walled Structures*, vol. 120, pp. 366–377, 2017.

[56] B. Riadh, A. H. Ait, A. Belqassim, T. Abdelouahed, and B. E. A. Adda, "Free vibration response of functionally graded porous plates using a higher-order shear and normal deformation theory," *Earthquakes Structures*, vol. 16, pp. 547–561, 2019.

[57] F. Ebrahimi and A. Jafari, "A higher-order thermomechanical vibration analysis of temperature-dependent FGM beams with porosities," *Journal of Engineering*, vol. 2016, Article ID 9561504, 20 pages, 2016.

[58] W. Gao, Z. Qin, and F. Chu, "Wave propagation in functionally graded porous plates reinforced with graphene platelets," *Aerospace Science and Technology*, vol. 102, Article ID 105860, 2020.

[59] R. Moradi-Dastjerdi and K. Behdinan, "Thermo-electro-mechanical behavior of an advanced smart lightweight sandwich plate," *Aerospace Science and Technology*, vol. 106, Article ID 106142, 2020.

[60] R. Moradi-Dastjerdi and K. Behdinan, "Temperature effect on free vibration response of a smart multifunctional sandwich plate," *Journal of Sandwich Structures and Materials*, Article ID 1099636220908707, 2020.

[61] R. Moradi-Dastjerdi, K. Behdinan, B. Safaei, and Z. Qin, "Buckling behavior of porous CNT-reinforced plates integrated between active piezoelectric layers," *Engineering Structures*, vol. 222, Article ID 111141, 2020.

[62] Ş. D. Akbaş, "Vibration and static analysis of functionally graded porous plates," *Journal of Applications and Computer Mechanics.*vol. 3, pp. 199–207, 2017.

[63] N. Wattanasakulpong and V. Ungbhakorn, "Linear and nonlinear vibration analysis of elastically restrained ends FGM beams with porosities," *Aerospace Science and Technology*, vol. 32, no. 1, pp. 111–120, 2014.

[64] F. Allahkarami, H. Tohidi, R. Dimitri, and F. Tornabene, "Dynamic stability of Bi-directional functionally graded porous cylindrical shells embedded in an elastic foundation," *Applied Sciences*, vol. 10, 2020.

[65] F. Fan, Y. Xu, S. Sahmani, and B. Safaei, "Modified couple stress-based geometrically nonlinear oscillations of porous functionally graded microplates using NURBS-based isogeometric approach," *Computer Methods in Applied Mechanics and Engineering*, vol. 372, Article ID 113400, 2020.

[66] I. Mechab, B. Mechab, S. Benaissa, B. Serier, and B. B. Bouiadjra, "Free vibration analysis of FGM nanoplate with porosities resting on Winkler Pasternak elastic foundations based on two-variable refined plate theories," *Journal of the Brazilian Society of Mechanical Sciences and Engineering*, vol. 38, no. 8, pp. 2193–2211, 2016.

[67] H. Shahverdi and M. R. Barati, "Vibration analysis of porous functionally graded nanoplates," *International Journal of Engineering Science*, vol. 120, pp. 82–99, 2017.

[68] M. R. Barati and H. Shahverdi, "Forced vibration of porous functionally graded nanoplates under uniform dynamic load using general nonlocal stress-strain gradient theory," *Journal of Vibration and Control*, vol. 24, no. 20, pp. 4700–4715, 2017.

[69] D. Shahsavari, B. Karami, H. R. Fahham, and L. Li, "On the shear buckling of porous nanoplates using a new size-dependent quasi-3D shear deformation theory," *Acta Mechanica*, vol. 229, no. 11, pp. 4549–4573, 2018.

[70] A. A. Daikh, M. S. A. Houari, and A. Tounsi, "Buckling analysis of porous FGM sandwich nanoplates due to heat conduction via nonlocal strain gradient theory," *Eng. Res. Express.*vol. 1, p. 15022, 2019.

[71] S. Sahmani, A. M. Fattahi, and N. A. Ahmed, "Analytical treatment on the nonlocal strain gradient vibrational response of postbuckled functionally graded porous micro-/nanoplates reinforced with GPL," *Engineering with Computers*, vol. 36, no. 4, pp. 1559–1578, 2020.

[72] S. Coskun, J. Kim, and H. Toutanji, "Bending, free vibration, and buckling analysis of functionally graded porous microplates using a general third-order plate theory," *Journal of Composites Science*, vol. 3, no. 1, p. 15, 2019.

[73] P. V. Vinh, N. T. Dung, N. C. Tho, D. V. Thom, and L. K. Hoa, "Modified single variable shear deformation plate theory for free vibration analysis of rectangular FGM plates," *Structure*, vol. 29, pp. 1435–1444, 2021.

[74] H.-T. Thai and D.-H. Choi, "A simple first-order shear deformation theory for the bending and free vibration analysis of functionally graded plates," *Composite Structures*, vol. 101, pp. 332–340, 2013.

[75] H.-T. Thai and D.-H. Choi, "A simple first-order shear deformation theory for laminated composite plates," *Composite Structures*, vol. 106, pp. 754–763, 2013.